nature photonics

REVIEW ARTICLE

PUBLISHED ONLINE: 6 MARCH 2011 | DOI: 10.1038/NPHOTON.2011.15

Exciton–polariton light–semiconductor coupling effects

H. M. Gibbs[1]*, G. Khitrova[1] and S. W. Koch[2]

The integrated absorption of an excitonic resonance is a measure of a semiconductor's coupling to an optical field. The concept of an exciton–polariton expresses the non-perturbative coupling between the electromagnetic field and the optically induced matter polarization. Ways to alter this coupling include confining the light in optical cavities and localizing the excitonic wavefunction in quantum wells and dots, which is illustrated by quantum strong coupling between a single dot and an optical nanocavity. Positioning quantum wells in periodic or quasiperiodic lattices with spacing close to a half wavelength results in pronounced modifications to the light transmission. Light–matter coupling can also be used to generate and interrogate an exciton population, for example by the recently developed technique of absorbing terahertz radiation.

Semiconductors and their nanostructures exhibit many fascinating features that are attributable to their intricate light–matter coupling properties. The response of a material to a weak field, known as its linear optical response, is governed by the transition amplitude of an electron from the valence band to the conduction band. The missing valence-band electron — the hole — is a quasiparticle with positive charge that experiences an attractive Coulomb interaction with the negatively charged conduction-band electron. The resulting pair state, commonly referred to as the (Wannier) exciton, has a binding energy ranging from a few millielectronvolts to a hundred millielectronvolts, giving rise to resonances in the optical spectrum that are energetically well below the fundamental absorption edge (that is, below the bandgap of the unexcited material). Hence, the linear optical semiconductor properties are inherently governed by Coulombic interaction effects.

From Maxwell's equations, we know that an electromagnetic field interacts with a charge-neutral dielectric medium, such as a semiconductor, through the optically induced dipoles commonly described by the material's polarization. Because the electromagnetic field and polarization are both characterized by amplitude and phase, we refer to them as coherent fields, in contrast with optically incoherent quantities such as light intensity or carrier populations, which have no phase information. The imaginary part of the polarization determines the optical absorption spectrum, which exhibits strong excitonic resonances, whereas the real part determines the optically induced refractive index changes.

In 1958, John Hopfield noted in his groundbreaking paper[1] that the fundamental optical absorption process is not a conversion of photons into excitons but rather a two-stage process with excitons (we refer to this state as the excitonic polarization) as an intermediate step; that is, the electromagnetic field induces an excitonic polarization that can then be converted into a population by the interaction processes. Hopfield introduced the term 'polariton' to denote the coupled light and polarization fields that form a mixed-mode excitation in a semiconductor system.

Because the original analysis by Hopfield focused on bulk semiconductor systems, the inclusion of spatial dispersion made it necessary to introduce 'additional boundary conditions'[2,3] to match the single incoming electromagnetic field at the semiconductor–air interface with the two propagating polariton modes inside the material. The boundary conditions were introduced in an *ad hoc* fashion that allowed for different choices, making this explanation highly controversial[4–7] until a proper solution was obtained[8] through a fully self-consistent space–time-dependent calculation of the propagating fields coupled to the inhomogeneous excitonic polarization.

Polaritons are intrinsically a concept of a linear system, and it was noted[9,10] quite early on that a polariton-based analysis of excitonic laser processes in bulk semiconductors allows for a simplified modelling of experimentally observed features. Owing to the severely limited numerical resources of the 1970s, these treatments often had to resort to poorly controlled approximations, such as the treatment of excitons as interacting Bosons by ignoring the fundamental Fermionic features of the constituent electrons and holes. Such simplified models are sometimes used even today and may allow for interesting insights, although often at the expense of full theoretical consistency. A systematic treatment of light–matter interaction effects can be achieved by microscopically describing electron–hole pair excitations, their many-body interactions and how they couple to the light field[11–14]. In such an analysis, polariton features appear automatically through the self-consistent treatment of the light–matter interaction.

Although Hopfield originally introduced the polariton concept for bulk semiconductors, it is by no means limited to these structures. Exciton polaritons are also important for describing the light–matter coupling in quantum well (QW) lattices and in planar microcavities containing QWs, as we will discuss in the following sections.

Tailoring the light–matter coupling

Owing to their mixed-mode nature, polariton features can be manipulated by changing either the excitonic properties or the optical eigenmodes of the system; ideally one wants to optimize both simultaneously. High-quality low-dimensional semiconductor systems are often introduced into dielectrically structured environments for this purpose.

One of the main reasons for choosing low-dimensional semiconductors rather than bulk material is because the excitonic binding energy — and thus the oscillator strength of the resonance — increases with decreasing system dimensionality. Whereas an ideal two-dimensional (2D) exciton is four times as strongly bound as its 3D counterpart[15], the exciton binding in a strictly 1D system is

[1]College of Optical Sciences, The University of Arizona, 1630 E. University Blvd., Tucson, Arizona 85721-0094, USA. [2]Department of Physics and Material Sciences Center, Philipps-Universität Marburg, Renthof 5, D-35032 Marburg, Germany. *e-mail: hyattgibbs@att.net

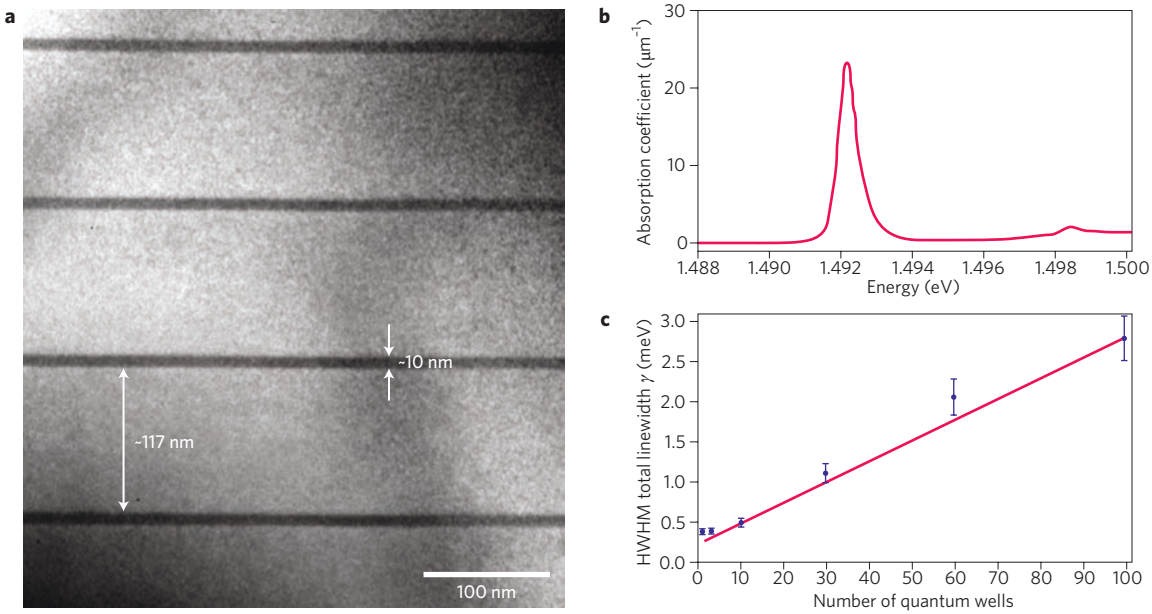

Figure 1 | MBE and narrow-linewidth excitonic transitions. Using MBE to grow semiconductor layers with almost monolayer precision has resulted in narrow-linewidth excitonic transitions that enhance the light–matter coupling needed for creating pronounced exciton–polariton effects. **a**, Transmission electron microscopy image of four $In_{0.04}Ga_{0.96}As$ QWs separated by GaAs barriers. **b**, Absorption coefficient per QW for 30 $In_{0.04}Ga_{0.96}As$/GaAs QWs with a 0.56 meV FWHM heavy-hole exciton linewidth. **c**, Reflectivity linewidth as a function of number of QWs, with the Bragg separation ($\lambda/2$) between QWs and with the top and bottom of the sample coated in an antireflective layer. The points are experimental linewidths with error bars depicting 10% uncertainty. The slope of the straight line yields 27 ± 2 μeV for the radiative damping rate of a single QW.

infinitely strong[16]. Because real structures are never truly 1D, no such divergence exists in nature. Although truly 2D systems also do not exist, high-quality QW structures based on GaAs-type materials show quasi-2D behaviour with strongly enhanced exciton effects. In quasi-0D quantum dot (QD) systems, the full motional quantization of electrons and holes leads to intrinsically discrete exciton states.

In addition to the enhancement of excitonic effects, low-dimensional semiconductor nanostructures have the significant advantage that they can be grown with very high quality using current state-of-the-art molecular beam epitaxy (MBE) techniques (Fig. 1a). Besides the controlled growth of individual structures, the introduction of passive separation (barrier or buffer) layers allows for a desired spatial arrangement and/or deposition onto prestructured material, such as high-quality mirrors (see below).

As always, problems may arise from the presence of undesirable imperfections such as growth inhomogeneities, which can lead to fluctuations in QW width or QD size. Furthermore, because binary, ternary or even quaternary material combinations must be used, a certain level of compositional fluctuation is practically unavoidable. All these features influence the spectral position and strength of the excitonic resonances that cause inhomogeneous broadening effects.

Although inhomogeneous broadening can be minimized by optimized growth, the interaction processes inherent to electronic semiconductor excitations are unavoidable. Before analysing these interactions and their influence on dephasing and exciton population formation in more detail, it is important to discuss how the resonant eigenmodes are tailored by dielectrically structuring the semiconductor material.

According to Snell's law, light propagating through the interface between two media with dielectric constants n_1 and n_2 is partially reflected and partially transmitted. If two or more of such interfaces are present, then interference also occurs between the multiply reflected/transmitted light beams. Constructive interference can lead to very high reflectivity, for example in a distributed Bragg reflector (DBR), which consists of alternating materials that each have an optical path length (refractive index n times the physical length) a quarter of the vacuum wavelength λ_v. Each partial reflection is in phase, resulting in a total reflectivity that approaches unity as the number of interfaces becomes very large. Two such DBRs, separated by a spacer whose thickness is an integer multiple of half-wavelengths, forms a planar microcavity — a Fabry–Pérot interferometer with an extension of a few optical wavelengths (Fig. 2a). The quality factor Q of the cavity is very high because the reflectivity of a DBR mirror is close to unity, which leads to strongly enhanced intracavity light fields (Fig. 2b).

The optical periodicity of the DBR allows it to be visualized as a 1D photonic crystal. Both 2D and 3D photonic crystal structures have also been demonstrated[17,18] and studied extensively. Etching periodic arrays of air holes into a planar semiconductor structure forms a 2D photonic crystal if the optical path length between the holes equals half the wavelength. 3D microcavities can be manufactured, using a half-wavelength-thick slab for vertical confinement through total internal reflection, simply by leaving out or shrinking the diameter of one or a few of the holes. Properly adjusting the size and arrangement of the holes around this defect allows for Q-factors exceeding one million[19]. As a consequence, the light-field amplitudes inside these 3D cavities are strongly enhanced over their 1D counterparts.

Utilizing total internal reflection in one, two or three dimensions — with a photonic crystal in the other two, one or zero dimensions — results in either a photonic crystal slab, micropillar and nanobeam, or microdisk 3D optical cavity, respectively. Except for the relatively new micropillar and nanobeam arrangement[20,21], these cavities are well-reviewed[22–24]. Photonic crystal slab cavities are emphasized in this Review because they are especially well-suited to planar integrated photonics. With one or more internal emitters, cavity design enables both the emission direction and the photon emission dynamics to be controlled[24,25].

Light–matter coupling in cavities

Placing high-quality QWs or layers of QDs at the antinodes of the intracavity light field leads to pronounced coupling

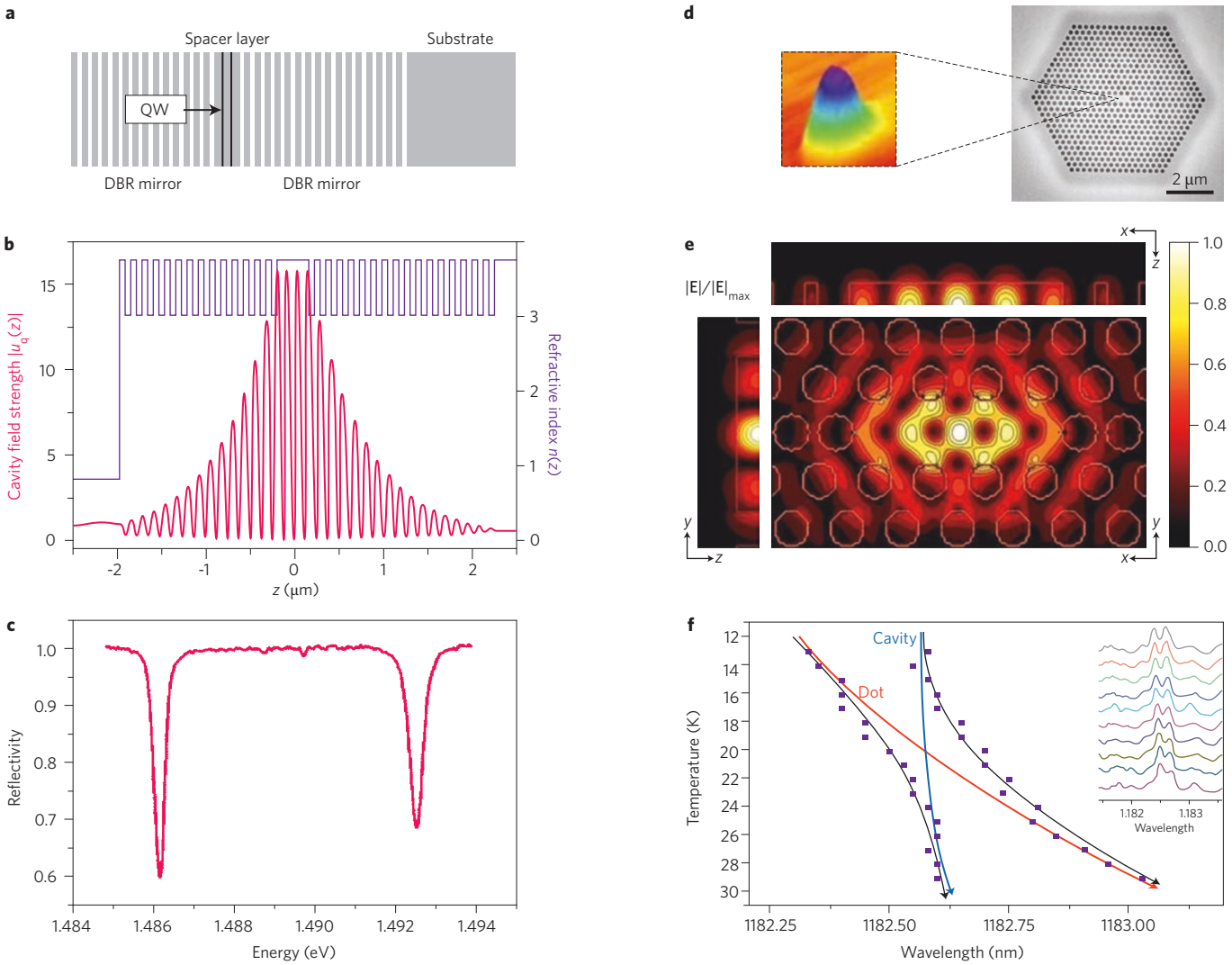

Figure 2 | Comparison between semi-classical normal-mode coupling of a QW in a planar microcavity and quantum vacuum Rabi splitting of a single QD in a photonic crystal slab nanocavity. a–c, QW planar microcavity vacuum Rabi splitting. **a**, Schematic of a planar microcavity consisting of two DBRs and a GaAs spacer layer with two QWs in the cavity-field antinodes. **b**, Computed position dependence of the cavity field strength $u_q(z)$ and the refractive index $n(z)$. **c**, Observed normal-mode coupling at zero detuning with ten QWs in a 5.5λ microcavity with mirrors designed for 99.94% reflectivity. **d–f**, Single QD photonic crystal slab nanocavity vacuum Rabi splitting. **d**, Scanning electron microscopy image of an L3 photonic crystal slab nanocavity with three missing holes forming the 'spacer'. The centre of the slab contains a plane of InAs QDs; an atomic force microscopy image of such a QD without a cap layer is shown on the left. **e**, Computed positional dependence of the cavity optical field. **f**, Plot of the photoluminescence peaks observed using temperature to scan the single QD transition through the cavity mode. Inset shows the photoluminescence spectra over the range 15 K (top) to 19.5 K (bottom).

effects if the exciton resonance energy coincides with that of a cavity eigenmode.

A strong matter resonance is needed to achieve such pronounced matter–field coupling, as discussed above. Because oscillator strength is conserved, a narrower linewidth provides a stronger resonance. Figure 1b displays the measured absorption coefficient per QW for InGaAs QWs often used in light coupling experiments, both in cavities and between multiple QWs[26,27]. The total linewidth is an order of magnitude larger than the radiative linewidth; this inhomogeneous broadening exists already in a single QW due to fluctuations in well thickness as a function of position within the probe beam. Growing such QWs in the antinodes of the field of a planar microcavity designed for low-temperature operation (as shown in Fig. 2a,b) provides strong coupling between the QW excitonic resonance and the cavity field. Weisbuch *et al.* were the first to observe this QW vacuum Rabi splitting, or 'normal mode coupling' as it is often called, emphasizing the analogy to any two coupled oscillators[28]. An example of normal mode coupling with a large splitting-to-linewidth ratio is shown in Fig. 2c[12]. The coupling of the induced excitonic polarization and the light field leads to cavity–exciton polaritons[28–30]. If the microcavity is excited resonantly with a pulse that is short compared with the cavity–exciton polariton decay time, emission oscillations are seen as the excitation goes back and forth between being light that can leak out of the cavity and being a material excitation, namely an excitonic polarization. The linear and nonlinear optical properties of planar microcavity normal mode coupling are summarized in two separate reviews[12,31].

Over the past decade, research on normal-mode coupling microcavities has split into the search for and study of the quantum regime, and investigations into the many-body coherence. One can test how far away a system is from the quantum regime by seeing how many photons it has to absorb before its spectrum changes; for a typical QW planar microcavity this is around 90 photons per

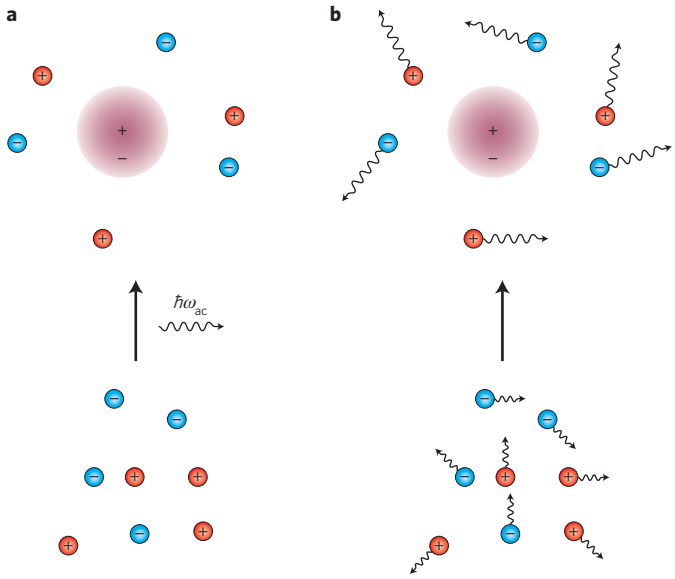

Figure 3 | Exciton formation mechanisms for low-energy carriers. **a**, Exciton formation through acoustic phonon emission (energy $\hbar\omega_{ac}$). **b**, Exciton formation through the many-body Coulomb interaction. The exciton binding energy is transferred to the electron–hole plasma, resulting in heating. The lengths of the wiggly arrows are proportional to the thermal velocity.

square micrometre[32]. Thus, for a typical probe beam of 50 μm diameter, the photon saturation number is almost 200,000; the observed vacuum Rabi splitting is then analogous to that observed in atomic experiments with a very large number of atoms[12,23]. Even in a photonic crystal slab nanocavity with a mode area of about 0.15 μm^2 at a wavelength of 1,200 nm (as shown in Fig. 2d), the saturation photon number for a QW active medium is about 13. Although this is likely to be an interesting regime with large statistical fluctuations, it will not be the true quantum regime, in which the absorption of a single photon changes everything, as in single-atom vacuum Rabi splitting[33–35]. The diameter of the semiconductor QW must therefore be even smaller than the mode diameter, which requires the use of a QD.

The photonic crystal approach to the quantum regime involves etching air holes into planar slab semiconductor structures containing layers of QDs, as depicted in Fig. 2d and described above. The lifetime (linewidth) of a typical self-organized InAs QD is a few nanoseconds (a few microelectronvolts)[36] — much longer than the photon decay time of 5–10 ps (~100 μeV). A 3D cavity polariton mode is formed if a QD is at a position of a high field amplitude (see the cavity mode profile in Fig. 2e) and its excitonic resonance coincides with the cavity eigenfrequency. Tuning the relative energies of the QD and cavity results in an anticrossing of the two resonances (Fig. 2f)[37]. This quantum strong coupling regime was first seen in a micropillar cavity[38] containing a larger QD than that used in ref. 37, with the larger dipole moment compensating for the larger mode volume, and was later seen in a microdisk cavity using an interface fluctuation QD of even larger dipole moment[39]. See ref. 23 for a comparison of these first three systems, and ref. 40 for the use of a microsphere.

The typical ratio between the vacuum Rabi splitting due to a single QD and the linewidth is not much larger than unity (Fig. 2f, inset). Despite considerable effort to improve this ratio, there have been few reports of success, and reproducibility is almost nonexistent. Nevertheless, several significant demonstrations have been reported. Photon statistics show that the emission from such a quantum strong coupling system is antibunched, thus verifying that a single QD is responsible for the splitting[41,42]. Such a device can be operated in a photon blockade mode for a probe beam resonant with the upper transmission peak; when the QD is unexcited, light is transmitted, and when the QD is excited, the probe is reflected. Consequently, the transmitted light is antibunched[43].

The regime of reduced photon loss will undoubtedly be pursued by improving fabrication techniques and investigating other material systems. Improving the ratio of the quantum vacuum Rabi splitting to the coupled system linewidth would, for example, enable more definitive demonstrations of single-QD lasing[44], higher rungs of the Jaynes–Cummings ladder[45] and single-photon switching through photon blockades[43]. This large ratio is also required by modalities that use quantum entanglement to achieve quantum state transfer. On the other hand, quantum strong coupling is not needed at all for many applications. The weak coupling regime with a large Purcell factor can efficiently couple light from an excited QD into the cavity mode and then out into free space or into an optical fibre. This regime is used to make quantum light sources[46] such as a photon turnstile (single photon on demand) or a continuous-wave source of antibunched light[46,47], sometimes with no Purcell enhancement[48]. It is also appropriate for realizing fast several-photon switches[49–51], QD lasers[52–54] and many other photonic devices[55].

The other main research direction that has grown out of investigations into normal mode coupling planar microcavities over the past decade is the search for many-body coherence. The first research surge involved pumping a normal-mode coupling planar microcavity at the 'magic angle', converting two pump photons into an idler photon and a signal photon (emitted normal to the cavity and at the lower branch wavelength), which conserves energy and momentum for the conversion[56,57]. From a practical point of view, this parametric amplification unfortunately requires a coherent pump that is stronger in intensity than (and close in wavelength to) the coherent output beam. For pumping away from the magic angle, generating either cavity-exciton polaritons resonantly at a very large angle[58,59] or carriers above band (which then must form excitons through a much slower process, as discussed below[60]), light emission with some degree of coherence has been reported at excitation densities an order of magnitude or two below those required for lasing using electron–hole–plasma gain[57,61]. Those authors claim that cavity-exciton polaritons undergo Bose–Einstein condensation to the lowest state, which then emits coherent light. Here we do not analyse such cases theoretically, and given the availability of long reviews on the subject[57,59,62] we choose not to cover reports of superfluidity, quantized vortices and Bose–Einstein condensation of exciton polaritons in planar microcavities.

Light–matter coupling in QW lattices

Strong polaritonic effects can also result from a lattice of many QWs without a cavity. QW excitonic resonances are especially well-suited for forming polaritonic systems, for a number of reasons. First, the QW thickness (~8 nm) is much thinner than half of a typical wavelength λ in the material ($\lambda_v/2n$ ~ 115 nm). Thus, the Bragg condition for maximum reflectivity — that the QWs are $\lambda/2$ apart so the fields emitted backwards by the QW polarizations are all in phase — is easily satisfied. Second, MBE growth is capable of positioning the QWs at an accuracy much less than the QW thickness (Fig. 1a). Third, the total linewidth of the excitonic resonance in high-quality samples is small enough (~0.5 meV) that radiative coupling (polaritonic) effects can dominate with a reasonable number N of QWs (10–100) that can be grown practically by MBE.

It was predicted early on[63,64] that a clear signature of inter-QW radiative coupling is the system reflectivity linewidth of $N\Gamma_0$ at Bragg spacing, where Γ_0 is the full-width at half-maximum (FWHM) radiative linewidth of a single QW. Typically, Γ_0 = 50 μeV for a high-quality $In_{0.04}Ga_{0.96}As/GaAs$ QW[12,27]. This linear dependence on the reflection linewidth has been demonstrated for $N < 100$, with peak reflectivities

exceeding 90% and FWHM linewidths reaching 5 meV — much larger than the inhomogeneous linewidth (0.5 meV) of a single QW (Fig. 1c). At Bragg spacing, all the oscillator strength of the N QWs goes into a single super-radiant mode of linewidth $N\Gamma_0$, whereas the other $N-1$ modes are dark. Correspondingly, in the time domain this Bragg-spaced coupling results in a very rapid decay of the polarization, as seen in four-wave mixing experiments[65]. Although changing the spacing slightly away from $\lambda/2$ allows other modes to gain oscillator strength and become bright, these modes lie close in frequency to the excitonic resonance.

Exciton–polariton dispersion curves can be measured by tilting the sample by an angle of θ and recording how the reflectivity or photoluminescence changes[66]. Just as for an empty cavity, the energy dispersion of the $\lambda/2$-spaced QWs changes in a $1/\cos\theta$ manner, which is much faster than the excitonic resonance dispersion. If one wants to interpret the dispersion curve in terms of an 'effective mass', the polariton effective mass is three or four orders of magnitude smaller than the exciton mass, just as it is for a cavity-exciton polariton. However, the effective mass concept must be used with some care, particularly given that the exciton polariton is a mixed mode combining intrinsically massless quasiparticles (photons) with massive quasiparticles (excitons).

Bragg-spaced periodic QWs are useful for contrasting polaritonic and emission properties. When excited non-resonantly, Bragg-spaced periodic QWs emit very poorly in the forwards and backwards directions, despite the fact that a resonantly excited polarization decays very rapidly in these directions[67]. Computing the electric field strength as a function of position throughout a periodic QW structure shows that the field nodes are centred on the QWs. Thus, recombination within the QWs couples very poorly to modes emitting perpendicular to the layers (vertically). Photoluminescence can occur at tilted angles, as the $1/\cos\theta$ dispersion removes the Bragg condition and the QWs are no longer at the field nodes. Similarly, vertical emission returns if the separation between QWs is altered from $\lambda/2$ (often accomplished experimentally by scanning across a gradient sample).

Note that in a multi-QW semiconductor laser the Fabry–Pérot resonances of the two Bragg mirrors and spacer can force field antinodes to form at the QW positions. All QWs are therefore optimally radiatively coupled for vertical emission. Even purely periodic QWs can simultaneously exhibit both passive dielectric and active excitonic periodic structures, provided the background refractive index of the QW is sufficiently different from that of the barriers between the QWs; this additional degree of freedom can be used to further control the emission properties of periodic QWs[68]. Alternatively, coupling a bulk excitonic resonance and a passive dielectric periodic structure results in two intergap modes, similar to the dispersion of a doublet of microcavity polaritons, giving rise to slow-light-enhanced nonlinear propagation and parametric scattering at two 'magic' frequencies[69].

QW lattices often result in sharp features in the reflection and transmission spectra that can be exploited for nonlinear optical switching schemes such as spin-dependent switching[70,71]. Commercial systems always use electro-optic switches because of their wavelength independence, cost and direct electrical control, but nonlinear optical switches continue to provide interesting studies of the underlying physics involved.

Semiconductor layers or QWs can also be positioned to form a 1D quasicrystal that possesses long-range order but lacks periodicity[72]. 1D photonic quasicrystals of both passive dielectrics and active excitonic resonances have so far been studied[73]. The long-range order gives a Bragg condition for maximum reflectivity, just as it does for periodic QWs. As one would expect, the peak reflectivity is lower and the linewidth is less broad than for an identical number of periodic QWs. The long-range order is introduced by positioning the QWs in a specific way. There are several ways of achieving this, but the one most studied for excitonic quasicrystals is based on the Fibonacci sequence.

When Fibonacci-spaced QWs are excited non-resonantly, the vertical photoluminescence intensity is unaffected by tuning through the Bragg condition, which is in sharp contrast with the deep minimum exhibited by periodic QWs[74]. This observation is consistent with the non-periodic spacing of the QWs; it is impossible for all of the QWs to be at nodes of the field. There are many similarities between Fibonacci-spaced QWs at the Bragg condition and periodic QWs slightly detuned from the Bragg condition, including sharp features that can be used for switching but disappear due to excitation dephasing as the carrier density increases[75].

Passive dielectric structures have been fabricated into 3D crystals and quasicrystals using direct laser writing[76] and interferometric[77] techniques. By loading such a structure with a dye, optically pumped lasing was observed that exhibited symmetry properties of the quasicrystalline host[77].

This section has emphasized light–matter coupling effects based on narrow-linewidth excitonic absorption. Although these effects are interesting and help us to learn more about the light-mediated coupling between QWs, they are not likely to result in practical applications because they are more pronounced at low temperatures and switching can be performed only when close to the excitonic resonance.

Interrogation of exciton populations

One approach that helps us to understand how the roles of electrons and holes contrast with those of exciton populations in highly excited light–matter systems is to develop a comprehensive many-body theory and compare it with definitive experiments. This approach has forced a reinterpretation of previous experimental conclusions.

As mentioned above, a resonant light field induces a coherent polarization at the excitonic eigenfrequency. Even in idealized, structurally perfect semiconductors, this excitonic polarization decays over time because of its coupling to the light field. Typical values for the radiative decay times in high-quality QWs are in the range of several to many picoseconds. However, at finite lattice temperatures, the polarization may also be destroyed by interactions with lattice phonons. Furthermore, if the system is excited beyond the linear regime, many-body interactions among the electron–hole excitations lead to intrinsic dephasing. This 'excitation-induced dephasing' was first identified as the dominant decay mechanism in four-wave mixing experiments[78] and as the reason for the gradual saturation of the exciton resonance in high-quality QWs without loss of oscillator strength[79].

The interaction processes may lead to the build-up of an incoherent excitonic population; that is, they provide a polarization-to-population conversion mechanism. However, because excitons are Coulomb-bound electron–hole pairs, the Fermionic nature of the constituents does not allow for arbitrarily high bound pair densities. The Fermi exchange interaction and the density-dependent screening of the attractive Coulomb potential together lead to a gradual weakening of the electron–hole binding, eventually causing a transition to a plasma state of unbound electrons and holes. This effect is often referred to as the excitonic Mott transition.

Even though excitonic effects are prominent in semiconductor optics, the unambiguous identification of exciton populations is not trivial. Because the appearance of a resonance in an absorption or luminescence spectrum merely demonstrates that the light–matter interaction is particularly strong at this frequency, the influence of populations on the interband optical effects is much more subtle. In fact, one must carefully evaluate how the different populations — that is, unbound electron–hole pairs and/or exciton populations — influence the spectra.

Pioneering work in this context was reported by Chatterjee *et al.*, who measured and analysed excitonic luminescence after non-

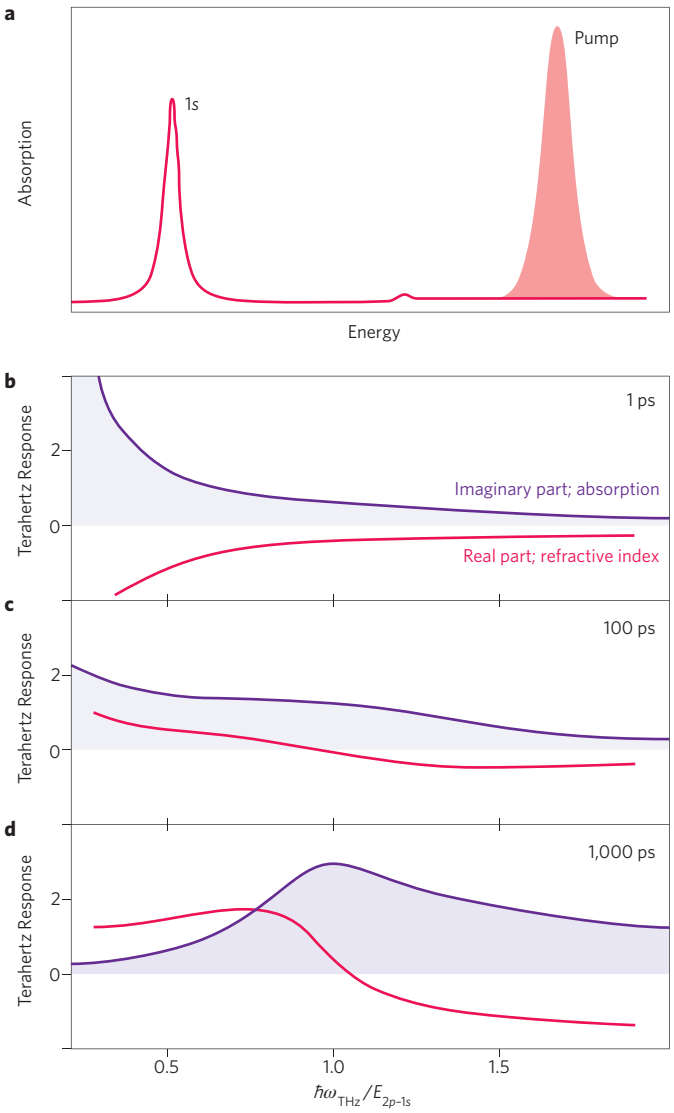

Figure 4 | Computed time-resolved terahertz spectra after optical interband excitation. a, Spectral position of the excitation relative to the exciton resonance. **b**, The terahertz spectrum at early times corresponds to a Drude response, which is characteristic for the plasma nature of the probed electron–hole pairs. **c**, Strong correlations build up on the 100 ps timescale. **d**, A clear 1s–2*p* transition emerges after 1 ns, indicating the formation of incoherent 1s–excitons.

resonant excitation using a microscopic many-body theory[80]. For the chosen interband excitation conditions, the induced optical interband polarization is rapidly converted into incoherent electron and hole populations. However, for sufficiently low temperatures and not too high densities, it may be energetically favourable for the system if some or all of the electrons and holes bind to excitons (Fig. 3). This exciton-formation process requires Coulomb- and optical-phonon-assisted carrier relaxation to the low-energy states of the conduction and valence bands and an interaction with acoustic phonons or the plasma to transfer the relatively small exciton binding energy from the electronic excitations to the lattice. Typical timescales for these processes are in the femto- to picosecond range for Coulomb and optical-phonon interactions, and in the nanosecond range for the acoustic-phonon-assisted conversion of unbound electrons and holes into excitons.

To monitor the appearance of excitonic populations, Chatterjee *et al.* performed detailed experimental investigations on high-quality QW samples by carefully monitoring the excitonic photoluminescence spectra and corresponding nonlinear absorption. Their analysis showed that pure plasma contributions are the luminescence source for slightly elevated lattice temperatures above 30 K, whereas for low densities and temperatures a contribution of exciton populations is required to fit the experimental results. These assignments are supported by time-resolved measurements showing different dynamical evolutions of the excitonic resonance and the continuum emission if excitons are formed, whereas the full spectrum shows uniform dynamics for the pure plasma case.

Terahertz spectroscopy is an alternative way of identifying populations of incoherent excitons. The most pronounced intra-excitonic terahertz resonance occurs at the energy corresponding to the exciton transition between the 1*s* and the 2*p* state[81,82]. In general, the 1*s*–2*p* peak in absorption can either originate from the coherent excitonic polarization or the incoherent 1*s*–exciton population[13,83]. Monitoring the appearance of this peak after interband excitation allows the exciton formation time to be determined. An example of the computed time-resolved terahertz spectra after non-resonant optical interband excitation is shown in Fig. 4. The results are in good qualitative agreement with experimental observations[84]. Figure 4 shows that the original terahertz spectrum roughly corresponds to a Drude response, which is characteristic for the plasma nature of the probed electron–hole pair. At later times — here after around 1 ns — a clear 1*s*–2*p* transition emerges, indicating the formation of incoherent 1*s*–excitons, which is in good qualitative agreement with photoluminescence results.

Quantitative optical measurements under resonant excitation conditions have recently been performed to detect subtle changes in the optical absorption spectra of QWs[85]. For the analysis, the optical response was calculated for more than 100,000 different electronic many-body states. The detailed comparison between quantitative experiments and theory shows that the absorptive nonlinearities depend so sensitively on the many-body configuration that the role of coherent polarization, exciton and electron–hole plasma contributions can be identified with great confidence. In the incoherent regime — that is, after the resonantly excited excitonic polarization has been converted into populations by the many-body interactions — one finds that nearly 100%-bound excitons are formed, as long as excitation densities are not too high. With increasing excitation level, the total electron–hole pair density first grows linearly as a function of excitation power, and then saturates. This is a consequence of excitation-dependent saturation of the 1*s*–exciton resonance, which strongly reduces the ability of the pump to generate more carriers. In parallel with this absorption saturation, the exciton fraction of the total electron–hole pair population decreases rapidly with increasing density because of induced ionization (the dynamic excitonic Mott transition). An alternative analysis of another experiment reaches different quantitative conclusions for resonant excitation[86]. However, the analysis is based on the questionable assumption of quasi-equilibrium between unbound electron–hole pairs and the excitons in all states, even though it is known that the optically active exciton states are strongly depleted because of the highly momentum-selective radiative emission process[87].

The complexity of simultaneous multiple interactions in a highly excited semiconductor coupled to optical field eigenmodes means that intuition often fails us. Prior to the computations described above and in refs 88–90, a photon emitted at the exciton resonance was interpreted as the signature of the decay of one member of the exciton population. Now we know that an electron and hole in a plasma can emit directly at the exciton energy by giving their excess energy and momentum to the other carriers that they are inescapably affecting through the Coulomb interaction (Fig. 3b). More than a decade ago it was shown that the luminescence from a normal-mode coupling planar microcavity is double peaked, with both peaks below the energy of the exciton continuum of the unexcited

QWs, even though the only excitations included in the theory were electrons and holes (that is, no exciton populations)[88]. To understand this finding it helps to distinguish between what causes the normal-mode splitting (the excitonic resonance in the light–matter coupling) and what gives rise to the luminescence (either an electron–hole pair or an exciton). This finding does not seem to be generally accepted, as two recent examples illustrate. In ref. 91 the appearance of an excitonic resonance in the luminescence spectrum is attributed only to the presence of an exciton population. In addition, the report[92] of a GaAs polariton LED operating near room temperature states: "the exciton and cavity modes are well-resolved over the entire temperature range, and exhibit the characteristic anticrossing behaviour of the strong coupling regime. This shows that electroluminescence in this intermediate temperature range arises unambiguously from exciton polariton states in the strong coupling regime, which is demonstrated for the first time in electrically pumped semiconductor microcavities." However, this report presents no unambiguous evidence that there are any excitons present or that exciton polariton states are formed; the same can be said about refs 93,94. As we have shown in our own work, the source of the luminescence could just as well be an electron–hole plasma, whereas the presence of double peaks only requires that most of the excitonic interband absorption features are still present.

Summary

The narrow exciton linewidths of QWs and QDs achieved by MBE growth lead to very pronounced light–matter coupling effects. MBE growth, electron beam lithography and various etching techniques are able to structure the dielectric environment of the QWs and QDs, thus defining light confinement eigenmodes. QWs spaced to produce a 1D photonic crystal or quasicrystal have interesting reflectivity and photoluminescence properties that are very different from randomly positioned QWs. Cavity eigenmodes close to an excitonic resonance give rise to cavity–exciton polaritons, which have been studied extensively in two modalities: with QWs, in efforts to generate coherent emission well below the threshold for plasma-gain lasing; and with a single QD, to reach the truly quantum regime of vacuum Rabi splitting for potential applications such as low-energy switches and sources of single photons on demand. To better understand cavity–exciton polaritons, it is also instructive to study exciton dynamics, in which the QW separations are chosen to suppress light coupling effects. Neither resonant nor non-resonant excitation generates a population of excitons instantaneously; both generate a polarization that scattering processes can convert into an exciton population or an electron–hole plasma, the ratio depending on the plasma temperature and the excitation density. Careful comparison between interband data and the many-body theory is able to determine the exciton population fraction, but monitoring the 1*s*–2*p* exciton transition with a terahertz probe is much more direct. Particularly promising research areas for the future are the terahertz probing and manipulation of exciton populations, cavity–exciton polariton coherent emission from semiconductors with very large exciton binding energies such as GaN[95,96] and organics[97], and quantum devices based on a single QD in a near-minimum-volume high-*Q* nanocavity.

References

1. Hopfield, J. J. Theory of the contribution of excitons to the complex dielectric constant of crystals. *Phys. Rev.* **112,** 1555–1567 (1958).
2. Pekar, S. I. The theory of electromagnetic waves in a crystal in which excitons are produced. *Soviet Phys. JETP* **6,** 785–796 (1958).
3. Hopfield, J. J. & Thomas, D. G. Theoretical and experimental effects of spatial dispersion on the optical properties of crystals. *Phys. Rev.* **132,** 563–572 (1963).
4. Henneberger, K. Additional boundary conditions: An historical mistake. *Phys. Rev. Lett.* **80,** 2889–2892 (1998).
5. Nelson, D. F. & Chen, B. Comment on 'Additional boundary conditions: An historical mistake'. *Phys Rev. Lett.* **83,** 1263–1263 (1999).
6. Zeyher, R. Comment on 'Additional boundary conditions: An historical mistake'. *Phys Rev. Lett.* **83,** 1264–1264 (1999).
7. Henneberger, K. Reply to comments on 'Additional boundary conditions: An historical mistake'. *Phys Rev. Lett.* **83,** 1265–1266 (1999).
8. Tignon, J. *et al.* Unified picture of polariton propagation in bulk GaAs semiconductors. *Phys. Rev. Lett.* **84,** 3382–3385 (2000).
9. Haug, H. & Koch, S. W. On the theory of laser action in dense exciton systems. *Phys. Stat. Sol. B* **82,** 531–543 (1977).
10. Koch, S. W., Haug, H., Schmieder, G., Bohnert, W. & Klingshirn, C. Stimulated intrinsic recombination processes in II–VI compounds. *Phys. Stat. Sol. B* **89,** 431–440 (1978).
11. Kira, M., Jahnke, F., Hoyer, W. & Koch, S. W. Quantum theory of spontaneous emission and coherent effects in semiconductor microstructures. *Prog. Quant. Electron.* **23,** 189–279 (1999).
12. Khitrova, G., Gibbs, H. M., Jahnke, F., Kira, M. & Koch, S. W. Nonlinear optics of normal-mode-coupling semiconductor microcavities. *Rev. Mod. Phys.* **71,** 1591–1639 (1999).
13. Kira, M. & Koch, S. W. Many-body correlations and excitonic effects in semiconductor. *Prog. Quant. Electron.* **30,** 155–296 (2006).
14. Haug, H. & Koch, S. W. *Quantum Theory of the Optical and Electronic Properties of Semiconductors* 5th edn (World Scientific, 2009).
15. Shinada, M. & Sugano, S. Interband optical transitions in extremely anisotropic semiconductors. I. Bound and unbound exciton absorption. *J. Phys. Soc. Japan* **21,** 1936–1946 (1966).
16. Loudon, R. One-dimensional hydrogen atom. *Am. J. Phys.* **27,** 649–655 (1959).
17. Krauss, T. F., De La Rue, R. M. & Brand, S. Two-dimensional photonic-bandgap structures operating at near infrared wavelengths. *Nature* **383,** 699–702 (1996).
18. Ho, K. M., Chan, C. T., Soukoulis, C. M., Biswas, R. & Sigalas M. Photonic band-gaps in 3-dimensions — new layer-by-layer periodic structures. *Solid State Commun.* **89,** 413–416 (1994).
19. Takahashi, Y. *et al.* High-*Q* nanocavity with a 2-ns photon lifetime. *Opt. Express* **15** 17206–17213 (2007).
20. Deotare, P., McCutcheon, M., Frank, I., Khan, M. & Loncăr, M. High quality factor photonic crystal nanobeam cavities. *Appl. Phys. Lett.* **94,** 121106 (2009).
21. Richards, B. *et al.* Characterization of 1D photonic crystal nanobeam cavities using curved microfiber. *Opt. Express* **18,** 20558–20564 (2010).
22. Vahala, K. J. Optical microcavities. *Nature* **424,** 839–846 (2003).
23. Khitrova, G., Gibbs, H. M., Kira, M., Koch, S. W. & Scherer, A. Vacuum Rabi splitting in semiconductors. *Nature Phys.* **2,** 81–90 (2006).
24. Shields, A. J. Semiconductor quantum light sources. *Nature Photon.* **1,** 215–233 (2007).
25. Purcell, E. M. Spontaneous emission probabilities at radio frequencies. *Phys. Rev.* **69,** 681–681 (1946).
26. Ell, C. *et al.* Influence of structural disorder and light coupling on the excitonic response of semiconductor microcavities. *Phys. Rev. Lett.* **80,** 4795–4798 (1998).
27. Prineas, J. P. *et al.* Exciton-polariton eigenmodes in light-coupled $In_{0.04}Ga_{0.96}As$/GaAs semiconductor multiple quantum well periodic structures. *Phys. Rev. B* **61,** 13863–13872 (1999).
28. Weisbuch, C., Nishioka, M., Ishikawa, A. & Arakawa, Y. Observation of the coupled exciton-photon mode splitting in a semiconductor quantum microcavity. *Phys. Rev. Lett.* **69,** 3314–3317 (1992).
29. Houdré, R. *et al.* Measurement of cavity-polariton dispersion curve from angle-resolved photoluminescence experiments. *Phys. Rev. Lett.* **73,** 2043–2046 (1994).
30. Andreani, L. C. & Panzarini, G. Polaritons in superlattices and in microcavities. *Nuovo Cimento. D* **17,** 1211–1218 (1995).
31. Skolnick, M. S., Fisher, T. A. & Whittaker, D. M. Strong coupling phenomena in quantum microcavity structures. *Semicond. Sci. Technol.* **13,** 1–25 (1998).
32. Lee, E. S. *et al.* Saturation of normal-mode coupling in aluminum-oxide-aperture semiconductor nanocavities. *J. Appl. Phys.* **89,** 807–809 (2003).
33. Thompson, R. J., Rempe, G. & Kimble, H. J. Observation of normal-mode splitting for an atom in an optical cavity. *Phys. Rev. Lett.* **68,** 1132–1135 (1992).
34. Kimble, H. J. Strong interactions of single atoms and photons in cavity QED. *Phys. Scripta* **76,** 127–137 (1998).
35. Kimble, H. J. The quantum internet. *Nature* **453,** 1023–1030 (2008).
36. Bayer, M. & Forchel, A. Temperature dependence of the exciton homogeneous linewidth in $In_{0.60}Ga_{0.40}As$/GaAs self-assembled quantum dots. *Phys. Rev. B* **65,** 041308 (2002).
37. Yoshie, T. *et al.* Vacuum Rabi splitting with a single quantum dot in a photonic crystal nanocavity. *Nature* **432,** 200–203 (2004).
38. Reithmaier, J. P. *et al.* Strong coupling in a single quantum dot-semiconductor microcavity system. *Nature* **432,** 197–200 (2004).
39. Peter, E. *et al.* Exciton photon strong-coupling regime for a single quantum dot in a microcavity. *Phys. Rev. Lett.* **95,** 067401 (2005).

40. Le Thomas, N. *et al.* Cavity QED with semiconductor nanocrystals. *Nano Lett.* **6,** 557–561 (2006).
41. Hennessy, K. *et al.* Quantum nature of a strongly coupled single quantum dot-cavity system. *Nature* **445,** 896–899 (2007).
42. Press, D. *et al.* Photon antibunching from a single quantum-dot-microcavity system in the strong coupling regime. *Phys. Rev. Lett.* **98,** 117402 (2007).
43. Faraon, A. *et al.* Coherent generation of non-classical light on a chip via photon-induced tunnelling and blockade. *Nature Phys.* **4,** 859–863 (2008).
44. Nomura, M., Kumagai, N., Iwamoto, S., Ota, Y. & Arakawa, Y. Laser oscillation in a strongly coupled single-quantum-dot-nanocavity system. *Nature Phys.* **6,** 279–283 (2010).
45. Kasprzak, J. *et al.* Up on the Jaynes-Cummings ladder of a quantum dot-microcavity system. *Nature Mater.* **9,** 304–308 (2010).
46. Strauf, S. Towards efficient quantum sources. *Nature Phys.* **4,** 132–134 (2010).
47. Englund, D. *et al.* Controlling the spontaneous emission rate of single quantum dots in a two-dimensional photonic crystal. *Phys. Rev. Lett.* **95,** 013904 (2005).
48. Claudon, J. *et al.* A highly efficient single-photon source based on a quantum dot in a photonic nanowire. *Nature Photon.* **4,** 174–177 (2010).
49. Nozaki, K. *et al.* Sub-femtojoule all-optical switching using a photonic-crystal nanocavity. *Nature Photon.* **4,** 477–483 (2010).
50. Miller, D. A. B. The role of optics in computing. *Nature Photon.* **4,** 406 (2010).
51. Mabuchi, H. Cavity-QED models of switches for attojoule-scale nanophotonic logic. *Phys. Rev. A* **80,** 045802 (2009).
52. Yoshie, T. O., Shchekin, B., Chen, H., Deppe, D. G. & Scherer, A. Quantum dot photonic crystal lasers. *Electron. Lett.* **38,** 967–968 (2002).
53. Hendrickson, J. *et al.* Quantum dot photonic-crystal-slab nanocavities: quality factors and lasing. *Phys. Rev. B* **72,** 193303 (2005).
54. Ulrich, S. M. *et al.* Photon statistics of semiconductor microcavity lasers. *Phys. Rev. Lett.* **98,** 043906 (2007).
55. Notomi, M. Manipulating light with strongly modulated photonic crystals. *Rep. Prog. Phys.* **73,** 096501 (2010).
56. Savvidis, P. G. *et al.* Angle-resonant stimulated polariton amplifier. *Phys. Rev. Lett.* **84,** 1547–1550 (2000).
57. Keeling, J., Marchetti, F., Szymanska, M. & Littlewood, P. Collective coherence in planar semiconductor microcavities. *Semicond. Sci. Technol.* **22,** R1–R26 (2007).
58. Deng, H., Weihs, G., Santori, C., Bloch, J. & Yamamoto, Y. Condensation of semiconductor microcavity exciton polaritons. *Science* **298,** 199–202 (2002).
59. Deng, H., Haug, H. & Yamamoto, Y. Exciton-polariton Bose-Einstein condensation. *Rev. Mod. Phys.* **82,** 1489–1537 (2010).
60. Kasprzak, J. *et al.* Bose-Einstein condensation of exciton polaritons. *Nature* **443,** 409–414 (2006).
61. Kasprzak, J. *et al.* Second-order time correlations within a polariton Bose-Einstein condensate in a CdTe microcavity. *Phys. Rev. Lett.* **100,** 067402 (*2008*).
62. Kavokin, A. Exciton-polaritons in microcavities cavities: Recent discoveries and perspectives. *Phys. Stat. Sol. B* **247,** 1898–1906 (2010).
63. Ivchenko, E. L. Exciton polaritons in periodic quantum-well structures. *Sov. Phys. Sol. State* **33,** 1344–1346 (1991).
64. Ivchenko, E. L. *Optical Spectroscopy of Semiconductor Nanostructures* Ch. 3, 338 (Alpha Science, 2005).
65. Kuhl, J. *et al.* Superradiant exciton/light coupling in semiconductor heterostructures – II: Experiments. *Adv. Sol. State Phys.* **38,** 281–295 (1999).
66. Mintsev, A. V. *et al.* Polariton dispersion of periodic quantum well structures. *JETP Lett.* **76,** 637–640 (2002).
67. Hübner, M. *et al.* Optical lattices achieved by excitons in periodic quantum structures. *Phys. Rev. Lett.* **83,** 2841–2844 (1999).
68. Goldberg, D. *et al.* Exciton-lattice-polaritons in multiple-quantum-well based photonic crystals. *Nature Photon.* **3,** 662–666 (2009).
69. Biancalana, F., Mouchliadis, L., Creatore, C., Osborne, S. & Langbein, W. Microcavity polariton-like dispersion doublet in resonant Bragg gratings. *Phys. Rev. B* **80,** 121306 (2009).
70. Johnston, W. J. *et al.* All-optical spin-dependent polarization switching in Bragg-spaced quantum well structures. *Appl. Phys. Lett.* **87,** 101113 (2005).
71. Yang, Z. S., Kwong, N. H., Binder, R. & Smirl, A. L. Stopping, storing, and releasing light in quantum-well Bragg structures. *J. Opt. Soc. Am. B* **22,** 2144–2156 (2005).
72. Janot, C. *Quasicrystals* 22–47 (Clarendon Press, 1994).
73. Poddubny, A. N. & Ivchenko, E. L. Photonic quasicrystalline and aperiodic structures. *Physica E* **42,** 1871–1895 (2010).
74. Hendrickson, J. *et al.* Excitonic polaritons in Fibonacci quasicrystals. *Opt. Express* **16,** 15382–15387 (2008).
75. Werchner, M. *et al.* One dimensional resonant Fibonacci quasicrystals: Noncanonical linear and canonical nonlinear effects. *Opt. Express* **17,** 6813–6828 (2009).
76. Deubel, M. *et al.* Direct laser writing of three-dimensional photonic-crystal templates for telecommunications. *Nature Mater.* **3,** 444–447 (2004).
77. Kok, M. H., Lu, W., Tam, W. Y. & Wong, G. K. L. Lasing from dye-doped icosahedral quasicrystals in dichromate gelatin emulsions. *Opt. Express* **17,** 7275–7284 (2009).
78. Wang, H. *et al.* Transient optical response from excitation induced dephasing in GaAs. *Phys. Rev. Lett.* **71,** 1261–1264 (1993).
79. Jahnke, F. *et al.* Excitonic nonlinearities of semiconductor microcavities in the nonperturbative regime. *Phys. Rev. Lett.* **77,** 5257–5260 (1996).
80. Chatterjee, S. *et al.* Excitonic photoluminescence in semiconductor quantum wells: Plasma versus excitons. *Phys. Rev. Lett.* **92,** 067402 (2004).
81. Groeneveld, R. M. & Grischkowsky, D. Picosecond time-resolved far-infrared experiments on carriers and excitons in GaAs-AlGaAs multiple-quantum wells. *J. Opt. Soc. Am. B* **11,** 2502–2507 (1994).
82. Cerne, J. *et al.* Terahertz dynamics of excitons in GaAs/AlGaAs quantum wells. *Phys. Rev. Lett.* **77,** 1131–1134 (1996).
83. Kira, M. & Koch, S. W. Exciton-population inversion and terahertz gain in resonantly excited semiconductors. *Phys. Rev. Lett.* **93,** 076402 (2004).
84. Kaindl, R. A., Carnahan, M. A., Hägele, D., Lovenich, R. & Chemla, D. S. Ultrafast terahertz probes of transient conducting and insulating phases in an electron-hole gas. *Nature* **423,** 734–738 (2003).
85. Smith, R. P. *et al.* Extraction of many-body configurations from nonlinear absorption in semiconductor quantum wells. *Phys. Rev. Lett.* **104,** 247401 (2010).
86. Kaindl, R. A., Hägele, D., Carnahan, M. A. & Chemla, D. S. Transient terahertz spectroscopy of excitons and unbound carriers in quasi-two-dimensional electron-hole gases. *Phys. Rev. B* **79,** 045320 (2009).
87. Siggelkow, S., Hoyer, W., Kira, M. & Koch, S. W. Exciton formation and stability in semiconductor heterostructures. *Phys. Rev. B* **69,** 073104 (2004).
88. Kira, M. *et al.* Quantum theory of nonlinear semiconductor microcavity luminescence explaining "boser" experiments. *Phys. Rev. Lett.* **79,** 5170–5173 (1997).
89. Kira, M., Jahnke, F. & Koch, S. W. Microscopic theory of excitonic signatures in semiconductor photoluminescence. *Phys. Rev. Lett.* **81,** 3263–3266 (1998*)*.
90. Kira, M., Hoyer, W., Stroucken, T. & Koch, S. W. Exciton formation in semiconductors and the influence of a photonic environment. *Phys. Rev. Lett.* **87,** 176401 (2001).
91. Kappei, L., Szczytko, J., Morier-Genoud, F. & Deveaud, B. Direct observation of the Mott transition in an optically excited semiconductor quantum well. *Phys. Rev. Lett.* **94,** 147403 (2005).
92. Tsintzos, S. I., Pelekanos, N. T., Konstantinidis, G., Hatzopoulos, Z. & Savvidis, P. G. A. GaAs polariton light-emitting diode operating near room temperature. *Nature* **453,** 372–375 (2008).
93. Khalifa, A. A., Love, A. P. D., Krizhanovskii, D. N., Skolnick, M. S. & Roberts, J. S. Electroluminescence emission from polariton states in GaAs-based semiconductor microcavities. *Appl. Phys. Lett.* **92,** 061107 (2008).
94. Bajoni, D. *et al.* Polariton light-emitting diode in a GaAs-based microcavity. *Phys. Rev. B* **77,** 113303 (2008).
95. Christmann, G., Butte, R., Feltin, E., Carlin, J.-F. & Grandjean, N. Room temperature polariton lasing in a GaN/AlGaN multiple quantum well microcavity. *Appl. Phys. Lett.* **93,** 051102 (2008).
96. Levrat, J. *et al.* Pinning and depinning of the polarization of exciton-polariton condensates at room temperature. *Phys. Rev. Lett.* **104,** 166402 (2010).
97. Kéna-Cohen, S. & Forrest, S. R. Room-temperature polariton lasing in an organic single-crystal microcavity. *Nature Photon.* **4,** 371–375 (2010).

Acknowledgements

H.M. Gibbs and G. Khitrova thank D. Gerthsen and D. Litvinov for the transmission electron microscopy image in Fig. 1a, and acknowledge support from the National Science Foundation, under AMOP (PHY-0757707), EPDT (ECCS-0757975) and ERC CIAN (EEC-0812072); AFOSR (FA9550-10-1-0003); and JSOP (W911NF-10-1-0344). S.W. Koch acknowledges stimulating and ongoing collaborations with M. Kira.

Additional information

The authors declare no competing financial interests.